ACS APPLIED MATERIALS & INTERFACES

www.acsami.org
Research Article

Thin, Uniform, and Highly Packed Multifunctional Structural Carbon Fiber Composite Battery Lamina Informed by Solid Polymer Electrolyte Cure Kinetics

Mohamad A. Raja, Su Hyun Lim, Doyun Jeon, Sangyoon Bae, Woong Oh, Inyeong Yang, Dajeong Kang, Jawon Ha, Ha Eun Lee, Il-Kwon Oh, Sanha Kim, and Seong Su Kim*

Cite This: ACS Appl. Mater. Interfaces 2024, 16, 59128−59142
Read Online

ACCESS | Metrics & More | Article Recommendations | Supporting Information

ABSTRACT: Multifunctional structural batteries promise advancements in structural energy storage technologies by seamlessly integrating load-bearing and energy-storage functions within a single material, reducing weight, and enhancing safety. Yet, commercialization faces challenges in materials processing, assembly, and design optimization. Here, we report a systematic approach to develop a carbon fiber (CF)-based structural battery impregnated with epoxy-based solid polymer electrolyte (SPE) via robust vacuum-assisted compression molding (VACM). Informed by cure kinetics, SPE processing enhances the multifunctional performance with no fillers or additives. The thin flexible CF-based laminae impregnated under high pressure achieved a substantial enhancement of ∼160% in the fiber volume fraction (FVF) as although thin and strip-shaped, the fibers were optimally packed with low void. A CF/SPE-based battery was fabricated, with a hybrid layered ionic liquid (IL)/carbonate electrolyte (CE) showing enhanced safety and multifunctional performance. Enhanced by thin, uniform, and stiff CF-based composites, this study propels the development of advanced multifunctional structures, thereby expediting sustainable commercialization.

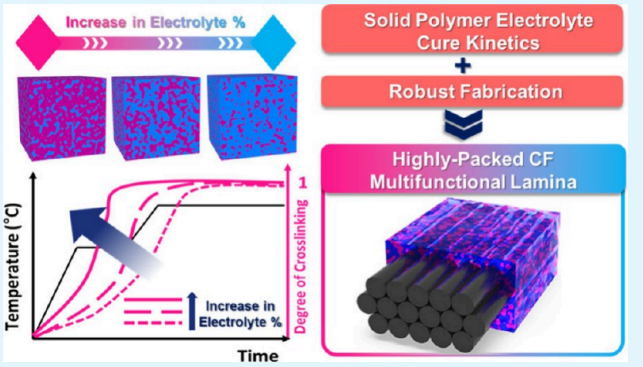

KEYWORDS: *multifunctional composites, carbon fiber battery, solid polymer electrolyte (SPE), functional materials, structural battery, smart polymer cure kinetics*

1. INTRODUCTION

Today's electrochemical energy storage devices face limitations in innovative applications in the biomedical, robotic, aerospace, and automotive industries due to restricted capacity, increased footprint, and safety risks. To enhance the efficiency of storage capacity, reduce the weight, and mitigate the risks, one approach is to leverage multifunctionality, employing structural elements as energy components to create structural batteries/supercapacitors.[1−5] In such a concept, energy storage and load-bearing capabilities are seamlessly integrated, thus facilitating mass saving with sacrificed performance compared to monofunctional constituents. For instance, CFs are renowned for their superior specific strength, stiffness, and design flexibility; consequently, they are heavily applied as reinforcement in structural composites. Nevertheless, they exhibit good electrical/thermal conductivities as well as electrochemical storage potential due to the inherent graphitic structure.[6−8] Therefore, in a multifunctional arrangement, CFs can serve as reinforcements, electrodes, and current collectors. Subsequently, to establish a structural electrochemical cell, CF layers are stacked and encapsulated with a solid-state electrolyte, enabling simultaneous ion conduction, load bearing, and fibers binding, synonymous with high-strength structural laminates.[9−11] In contrast to monofunctional constituents, the performance of multifunctional composites is inherently intertwined, leading to a trade-off relationship between the mechanical properties and electrochemical abilities. To address the lower capacity of pristine CFs and/or partially decouple the trade-off relationship, researchers often utilize CFs as skeletons or scaffolds with surface modifications. These modifications may include grafting of carbonaceous materials or metal−organic framework (MOF) functionalization[12−16] or the use of coated active materials.[17−20] However, such approaches are considered to operate at a lower level of multifunctionality, as CFs do not directly

Received: May 27, 2024
Revised: September 2, 2024
Accepted: September 3, 2024
Published: September 10, 2024

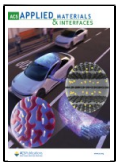

serve as electrodes (i.e., active materials), and they introduce various complications related to large-scale commercial production. To this extent, researchers have employed CFs as fully multifunctional components in previous research, exploring the effects of the sizing agent, precursor, tow density, and grade on the potential use in electrochemical applications.[21,22] While the evaluated cells were assembled by using a liquid electrolyte medium, thus diminishing their actual structural functions, others have synthesized structural batteries based on carbon fibers (CFs) impregnated with an epoxy-based solid polymer electrolyte (SPE). This approach leverages the excellent interfacial compatibility, high mechanical performance, and chemical resistance of epoxies,[23−25] compared to other weaker polymer-based electrolytes used in solid-state batteries (SSBs), such as poly(ethylene oxide) (PEO), poly(vinylidene fluoride) (PVDF), polyacrylonitrile (PAN), and poly(methyl methacrylate) (PMMA), as well as various dissolved lithium salts including $LiClO_4$, LiTFSI ($LiN(CF_3SO_2)_2$), $LiAsF_6$, and $LiPF_6$.[26,27] Thus, epoxy modified with liquid electrolyte has been used as a compromised solution for multifunctional polymer electrolyte systems for composite structural energy storage systems, where epoxy serves as a structural element providing simultaneous load transfer and bearing, while the electrolyte phase serves as an ion-conduction medium.

Nevertheless, the specific capacity and stiffness of all-functional structural batteries have been substantially lower than monofunctional devices, hindering the commercial realization due to shortcoming in (1) structural electrolyte processing, (2) CF lamina's morphological nonuniformity, and (3) assembly limitations dictated by the thermal stability and flammability of utilized electrolytes.

First, for structural battery's electrolytes, the limitation arises from not exploiting the utmost capabilities of epoxy-based solid electrolytes. To elaborate, the inclusion of a segregated electrolyte phase within the epoxy network significantly reduces the mechanical moduli, thereby diminishing its advantages. Furthermore, intricate processing, i.e., time, temperature, pressure, etc., becomes crucial, particularly when the integrated electrolyte phase relies on highly conductive but volatile, flammable, and thermally unstable organic electrolytes like DMC, DEC, PC, EMC, etc.[28,29] A detailed analysis regarding the electrolytes' safety and flammability can be found elsewhere.[30] Consequently, such aspects limit the cross-linking processing and the multifunctional performance of biphasic epoxy-based electrolytes. Especially that epoxy polymerization process requires high temperatures to achieve a robust and superior mechanical property, as well as this process is highly exothermic with temperature reaching up to 150 °C.[31] For instance, Carlstedt et al.[28] and Asp et al.[29] fabricated epoxy-based SPE by thermally curing at 90 °C for 60 min, while pressure was applied by office paper clamps, as EC:PC-based electrolyte was utilized. Therefore, safe, thermally, and chemically stable ionic liquid (IL) salts, with moderate ionic conductivity, and wide range of polymers compatibility have been an attractive alternative for structural batteries and supercapacitors.[17,32,33] Although various efforts have been explored such as adding organoclay, alumina, or carbon-based fillers to increase the diffusion paths,[33−35] such improvements were incremental. Furthermore, despite playing a paramount role in analyzing the effect of the cure cycle on polymer processing, impregnation, and overall performance, the epoxy-based SPE's cross-linking (i.e., curing) kinetics have not been explored, especially after incorporating the electrolyte phase.

Second, concerning the morphology, packing, and thickness uniformity of CF lamina, previous approaches have encountered issues such as irregular distributions, inconsistent thickness, and low fiber volume fraction (FVF). These challenges arise from processing restrictions imposed by the polymer electrolyte, as delicate procedures like inferior pressure, low temperature, and ultraviolet (UV) curing are necessary to ensure thermal stability and minimize flammability hazards of the volatile electrolyte phase, thus leading to loss of mechanical rigidity as well as unbalanced active material contact ratio which affects the intercalation distance and irreversible consumptions.[28,29,36,37] To that extent, Johannisson et al.[36] utilized UV curing to fabricate and impregnate SPE on CF, highlighting the presence of resin-rich layers on the edges of the thin CF lamina. This led to nonuniformity in lamina thickness, resulting in a mitigated fiber volume fraction (FVF) (i.e., 18%), decreased lamina stiffness, and increased internal transport pathways within the electrochemical cell.

Third, for assembly and fabrication considerations, IL-based electrolytes, although promising, have been proven to form unstable solid electrolyte interphase (SEI) on the electrode's surface. For example, Yun et al.[38] stated that this instability arises from the decomposition of the ionic liquid electrolyte, which hinders reversible electrochemical reactions, resulting in significant deterioration in electrochemical performance, especially during the initial cycling where the effects of SEI formation are substantial. Therefore, to improve the cycling stability of the IL-based electrolytes, SEI-forming additives such as anhydrous carbonates were deemed necessary to promote successful electrode protection from the reductive decomposition of the ionic liquid and enhancing the flammability resistance.[38,39]

In this work, to overcome the bottlenecks associated with structural batteries, we alleviate the aforementioned challenges via innovative materials processing, robust fabrication, and assembly methods. Specifically, by employing the following: (i) Cure kinetics informed cross-linking of thermally initiated biphasic epoxy/IL polymer electrolyte, showing an enhanced multifunctional polymer's capabilities (i.e., mechanical and electrochemical), to match those of similar monofunctional commercial constituents explored in previous research, without the need for additives. (ii) Fabrication of thin and highly uniform carbon fiber spread tow (CFST) lamina optimized by vacuum-assisted compression molding (VACM), achieving an unprecedented FVF with minimal voids, uniform thickness, and dense hexagonal morphological arrangement. The achieved FVF of 52% marked a significant rise of around 160% compared with prior studies on CF-based structural batteries. Moreover, the absence of significant thickness variations indicated high uniformity and packing, thereby enhancing the multifunctional performance. (iii) Assembly of a layered hybrid carbonate electrolyte (CE)/solid polymer electrolyte (SPE) electrolyte system was synthesized, referred to herein as CE|SPE, in which the separator was soaked in CE-based electrolyte, while in contact with SPE-impregnated CF lamina, showcasing improved thermal stability and safety compared to commercial systems. Mechanical tensile tests and galvanostatic charge−discharge (GCD) evaluations were performed on a multifunctional SPE-impregnated CF lamina, indicating the robust fabrication of CF-based structural batteries informed by cure kinetics as a pivotal approach. To

https://doi.org/10.1021/acsami.4c08698
ACS Appl. Mater. Interfaces 2024, 16, 59128−59142

Figure 1. Schematic illustration of the phase-segregated SPE showing the chemical structures of the mechanical and electrochemical constituents.

the best of the author's knowledge, such analyses have not been discussed or implemented before for multifunctional structural batteries or supercapacitors.

2. MATERIALS AND METHODS

2.1. Materials. Bifunctional SPEs were constructed from a structural phase consisting of bisphenol A diglycidyl ether epoxy resin (DGEBA; KUKDO Chemical, Korea), a cross-linking agent methylhexahydrophthalic anhydride (MHHPA; Sigma-Aldrich, Korea), and a catalyst *N*,*N*-dimethylbenzylamine (BDMA; Sigma-Aldrich, Korea). For the conducting electrolyte phase, commercially available 1-ethyl-3-methylimidazolium tetrafluoroborate ($EMIMBF_4$; Sigma-Aldrich, Korea) and lithium bis(trifluoromethanesulfonyl)-imide (LiTFSI; MTI, Korea) were utilized as solvent and solute, respectively. To prepare the CF-based multifunctional electrode, a unidirectional (UD) strip-shaped carbon fiber spread tows (T700 CFSTs length ∼100 mm and width ∼18 mm; Toray Industries Inc., Japan) laminae were used for mechanical/interfacial characterizations as well as electrochemical evaluations (Supporting Information, Figure S1). The CE electrolyte used in the layered CE|SPE arrangement consisted of ethylene carbonate (EC) and 1,2-dimethoxyethane (DME) (Sigma-Aldrich, Korea). The coin cells were based on CR2032 cells with a conventional layup. Half-cells were tested against lithium metal chips (diameter 16 mm, thickness 0.45 mm; MTI, Korea). A Whatman GF/A (thickness ∼260 μm; Sigma-Aldrich, Korea) glass fiber separator paper was used. Prior to assembly materials for electrochemical specimens (LiTFSI, separators, CF electrodes) were vacuum-dried at 100−120 °C for 24 h before usage. All other chemicals were used as received.

2.2. Biphasic Epoxy-Based Solid Polymer Electrolyte (SPE) Preparation. Anhydride-cured epoxy was chosen as the structural phase in the polymer electrolyte system due to its exceptional properties, including high thermal resistance (T_g), chemical resistance, long pot life, low cure shrinkage, and low cure exotherm. To prepare the structural phase, a stoichiometric resin-to-hardener mixing ratio of 100:90 parts per weight was used, with the addition of one part per weight of the accelerator. For the liquid electrolyte phase, 1 M LiTFSI was dissolved in $EMIMBF_4$ and then mixed with the structural epoxy phase based on specified weight percent ratios (i.e., 0%, 30%, 40%, and 50%) until a homogeneous mixture was achieved, denoted as SPE *X*, where *X* represents the electrolyte weight percent. Both the liquid electrolyte and the structural phases underwent vacuum drying at room temperature before and after mixing to eliminate any air and impurities. The biphasic epoxy-based SPE, illustrating the 3D connected mediums, is depicted in Figure 1.

2.2.1. Cure Kinetics Analysis of SPE. The cross-linking analysis of the solid polymer electrolyte (SPE) was conducted by analyzing the thermograms of the curing reaction using a TA Instruments DSC Q20. Approximately 10 mg of uncured SPE sample was weighed using a Mettler-Toledo balance (±0.1 mg) and placed in a hermetic aluminum pan (Tzero; TA Instruments, Switzerland). The experiments were carried out under a constant flow of nitrogen at a rate of 50 mL/min. Four isothermal temperatures were employed to study the curing reaction of the SPE: 80, 100, 130, and 140 °C, maintained for 300, 280, 250, and 140 min, respectively.

The degree of cure (i.e., degree of cross-linking), denoted as α, is correlated to the enthalpy released during the exothermic cross-linking reaction of the epoxy polymer. It can be determined by utilizing the partial heat of reaction at a specific time, represented as ΔH, and the total heat of reaction at $\alpha = 1$, calculated based on the maximum cured temperature, denoted as ΔH_T, as in eq 1.

$$\alpha = \frac{\Delta H}{\Delta H_T} \tag{1}$$

The time- and temperature-dependent fractional degree of cure, $\alpha(T,t)$, can be calculated during the curing reaction at different times using the differential form of the partial heat of reaction. The modified integral equation is shown in eq 2.

$$\alpha = \frac{1}{\Delta H_T}\int_0^t \left(\frac{dH}{dt}\right) dt \tag{2}$$

In this context, ΔH_T corresponds to the overall reaction heat, and dH/dt reflects the heat flow rate at time t. The rate of the cure can be calculated based on eq 3.

$$\frac{d\alpha}{dt} = \frac{1}{\Delta H_T}\frac{dH}{dt} \tag{3}$$

Throughout the curing process, various reactive phenomena unfold concurrently, encompassing gelation, vitrification, and the transition from chemical-driven to diffusion-driven conversion kinetics.[40,41] To deal with such challenges, different models have been proposed to describe the complex curing behavior of epoxy.[42−46] To analyze and model the cross-linking behavior of the formulated SPE, the widely used Kamal−Sourour model was applied as shown in eq 4.

$$\frac{d\alpha}{dt} = (K_1(T) + K_2(T)\alpha^m)(1-\alpha)^n \tag{4}$$

where K_1 and K_2 are specific rate constants and the parameters m and n are the overall reaction orders. All aforementioned parameters are temperature dependent, and the temperature dependence of the rate constants (i.e., K_1 and K_2) is given by the Arrhenius expressions in eq 5.

$$k_i = A_i e^{-E_i/RT};\ i = 1, 2 \tag{5}$$

where A_i denotes the pre-exponential factor, E_i represents the activation energy, R stands for the universal gas constant, and T is the reaction temperature.

The application of the cure cycle significantly impacts the performance and characteristics of the epoxy polymer. Typically, this influence is investigated using an autocatalytic reaction model, which describes the cross-linking rate as a function of time and temperature. Once validated with experimental data, this model can be broadly applied to various cure cycles for each epoxy formulation. Similarly, the cure analysis was applied to study the effect of the applied temperature cure cycle on the cross-linking rate and the maximum degree of cure (Figure S2) for both the SPE and the constituent epoxy phase as a benchmark comparison.

The glass transition temperature (T_g) was evaluated from the DSC analysis, where a fully cured sample of mass ∼10 mg was placed and sealed in hermetic aluminum similar to the aforementioned preparation procedure in the cure kinetics analysis. The samples were thermally scanned in a temperature range of 20−200 °C at a heating rate of 5 °C/min. The T_g is observed as an endothermic stepwise change in the DSC heat flow and characterized as T_g, onset, T_g, midpoint, and T_g, offset.

https://doi.org/10.1021/acsami.4c08698
ACS Appl. Mater. Interfaces 2024, 16, 59128−59142

Furthermore, the T_g is predicted using the Gordon−Taylor relation for mixtures, as shown in eq 6.

$$T_{g,SPE\_X} = \frac{(1 - \Phi_{SPE})T_g^{SPE\_0} + K\Phi_{SPE}T_g^{SPE\_100}}{(1 - \Phi_{SPE}) + K\Phi_{SPE}} \quad (6)$$

where T_{g,SPE_X} is the predicted T_g, Φ_{SPE} is the fraction of electrolyte in the polymer, $T_g^{SPE\_0}$ is T_g of the structural phase (i.e., 0% electrolyte), $T_g^{SPE\_100}$ is T_g of the electrolyte phase (i.e., 100% electrolyte),[47] and K is fitting constants dependent on the polymer composition.

2.3. Fabrication of CFST-Based Structural Battery Half-Cell. In this section, we present a proof-of-concept fabrication of a CF-based multifunctional lamina half-cell using a wet-layup process followed by vacuum-assisted compression molding (VACM). The manufacturing procedure proceeded as follows: The polymer was partially cured to a degree of cure (DOC) between 0.2 and 0.4, chosen for its handling feasibility, suitability for impregnation, and ensuring adequate cross-linking, following the validated cure cycle in Table 1. This process allowed the electrolyte to be trapped within the epoxy microstructure, preventing premature macro phase separation.

Table 1. Validated Cure Cycle Processing Conditions, Including Stepped Heating Rates and Dwellings

step	target temp (°C)	heating rate (°C/min)	time (h)
initial state	25		
first heating	90	6.5	
first dwell	90		2
second heating	130	4	
second dwell	130		1
third heating	150	4	
third dwell	150		2
natural cooling to room temperature (RT)			

Second, the SPE was coated into the carbon fiber spread tow strip using a resin spreader. Following coating, peel-ply, breather, release film, and vacuum bagging materials were applied to the assembly. Lastly, the validated cure cycle was employed, subjecting the assembly to extremely high pressure (around 110 bar) via an automatic hot-press heating plate (QM900A; QMESYS, Korea). This step ensured the formation of a lamina with a fully cross-linked polymer, uniform thickness, and morphology, resulting in an enhanced fiber volume fraction (FVF) as illustrated in Figure 2.

To validate the concept that VACM can yield a higher fiber packing arrangement with superior mechanical performance lamina, it was compared to the vacuum bag only (VBO) manufacturing method (i.e., same procedure but without the high pressure during vacuum processing) with the same applied cure cycle using a commercial epoxy for consistency.

2.4. Hybrid Electrolyte Mixture: Thermal Stability and Flammability. To evaluate the compatibility, thermal stability, and flammability of the fabricated electrolyte mixtures, various volumetric ratios of IL and the synthesized CE electrolyte were prepared. To evaluate the thermal stability, different solutions were mixed in small vials by a rotary vortex mixer. Then, it was dropped into the DSC sealing pan, where the masses were controlled to be <5 mg. DSC measurements were conducted under a N_2 atmosphere, heating the samples at a rate of 10 °C/min from 25 to approximately 160 °C. Flammability tests were conducted by igniting various electrolytes directly. Approximately 0.2 g of each electrolyte was dropped into a circular stainless-steel shell measuring 20 mm in diameter. Subsequently, a torch was used to ignite the electrolyte, while an infrared camera (IR; Fluke RSE600, USA) recorded both the intensity of combustion and the in situ thermogram. As a benchmark comparison, the fabricated electrolyte mixtures were compared to a widely used commercial electrolyte, i.e., $LiPF_6$ in EC:DMC:EMC (MTI, Korea).

2.5. Characterizations. *2.5.1. Materials Morphology Characterization.* To capture the morphology of the SPE, we cast stub samples in a 10 mm × 20 mm × 4 mm steel mold. The bicontinuous polymer structure of SPEs was analyzed using an AIS1800C scanning electron

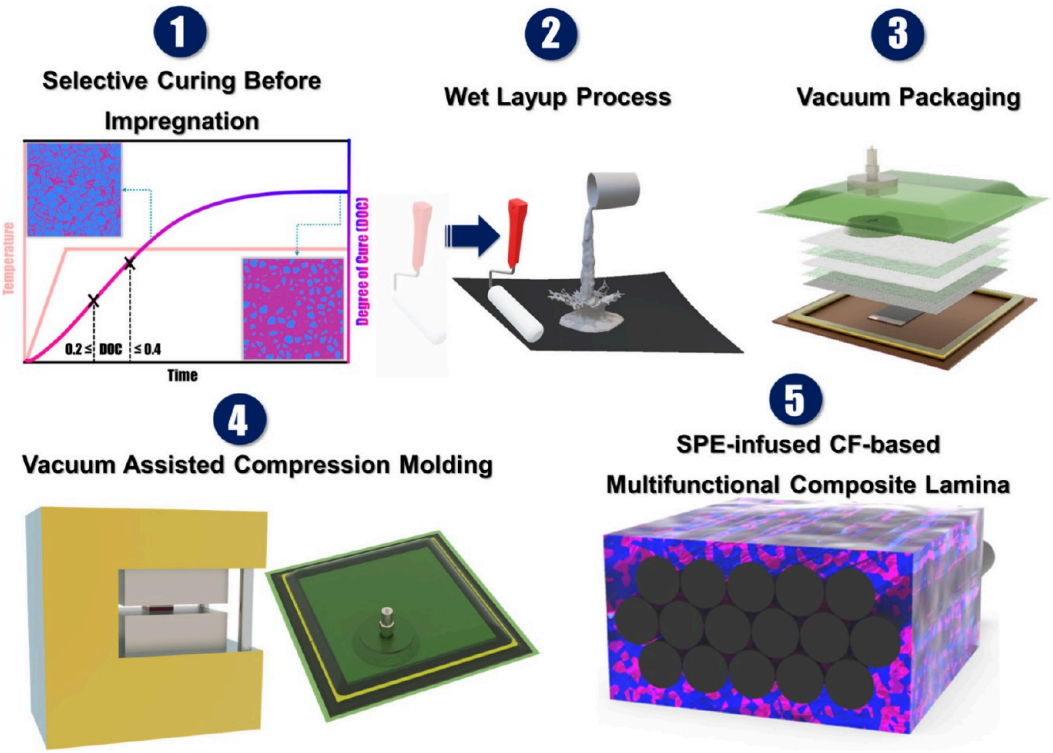

Figure 2. CF-based multifunctional lamina fabrication scheme informed by cure kinetics selective DOC curing and vacuum-assisted compression molding (VACM) under high pressure.

https://doi.org/10.1021/acsami.4c08698
ACS Appl. Mater. Interfaces 2024, 16, 59128−59142

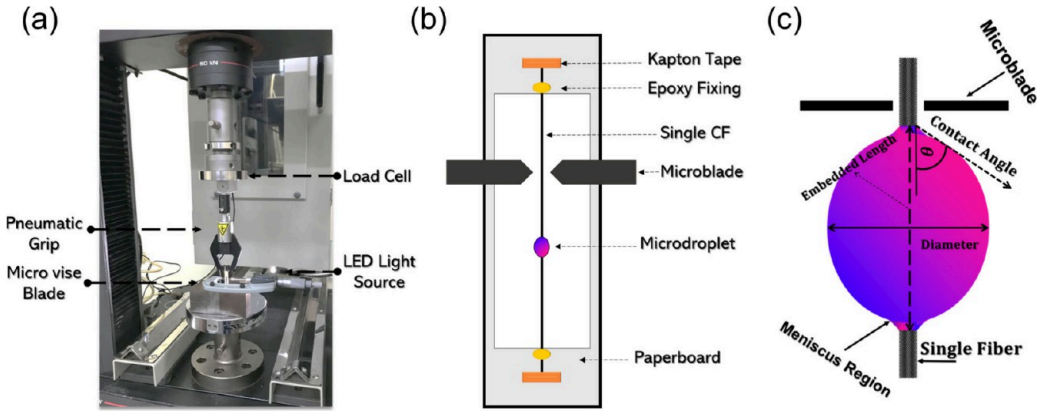

Figure 3. Illustrations of single carbon fiber and SPE interfacial test. (a) Experimental setup. (b) Specimen fixing layout on the substrate. (c) Typical geometry of a drop-on-fiber system and its parameters.

microscope (SEM, SERON, Korea). The procedure involved inspecting the sample's cross section subsequent to ethanol immersion for 2−3 days to extract the electrolyte phase. After extraction, the samples underwent overnight drying at 60 °C to eliminate residual ethanol, followed by rapid cooling in liquid nitrogen and sectioning with a sharp knife for cross-section analysis. Additionally, a Hitachi SU8230 field emission SEM (FE-SEM) at 10 kV was used to capture the CFST-impregnated-SPE morphology and determine the chemical elements present in the samples, along with their relative abundance, using built-in energy-dispersive X-ray spectroscopy (EDS). All samples were vacuum-dried before analysis. Furthermore, to estimate void analysis and analyze fiber arrangement in a single-layer CFST fabricated by VACM or VBO, a digital optical microscope (OM, VHX 700F, Keyence, Korea) was utilized. An in-house image processing MATLAB code was adopted, along with other analytical and experimental methods, to estimate the stochastic morphology of the VACM and VBO samples (Figure S3, eq S1, and eq S2). This highlighted the effect of high pressure on the sample's modulus, fiber volume fraction (FVF), fiber arrangement, void analysis, and fiber diameter.

2.5.2. Electrochemical Characterization. The ionic conductivity performance of SPE specimens was evaluated by using electrochemical impedance spectroscopy (EIS) analysis. The polymer sample, a disk with a 20 mm diameter and 2 mm thickness, was sandwiched between stainless steel electrodes coated with a thin film of conductive silver paste. As detailed in eq 7, the ionic conductivity was calculated by examining the Nyquist plot intersection point at the real axis and considering the dimensions of the polymer sample.

$$\sigma = \frac{t}{R_b A} \tag{7}$$

where t is the thickness, R_b is the resistance, and A is the area of contact. The experiment was performed at room temperature with a potential of 10 mV, covering a frequency range of 0.01 Hz−1 MHz. The equivalent circuit resistance and impedance of the polymer electrolytes were fitted and simulated using electrochemical software ZSimpWin, AMETEK, USA.

Electrochemical cells were assembled in an argon-filled glovebox with H_2O and O_2 concentrations maintained below 1 ppm. Gravimetric calculations for capacity and efficiency were based on CF-based anode mass.

The voltage limits of the half-cell were cycled between 0.002 and 1.5 V under constant current/constant voltage (CC/CV) protocol. Initially, the C-rate was based on the capacity of graphite (C = 372 mAh/g); however, as mentioned earlier, this may not accurately represent the actual capacity of CF. Therefore, the rated capacity was estimated based on the average of the initial 5 cycles of a pristine CF cell, and it was found to be approximately 105 mAh/g. The ambient room temperature (25 °C) during the battery tests was controlled with a thermal chamber (±0.3 °C) from JEIO TECH, Korea, and GCD tests were conducted using a WonATech automatic battery cycler. For reference, a cell without SPE (termed SPE 0, with CF as the anode and current collector only) was fabricated using the CE electrolyte for benchmark comparison.

2.5.3. Mechanical Tensile Testing. The tensile properties of the biphasic SPE were evaluated according to ASTM D638.[48] In this setup, a woven GFRP handle (i.e., grip) was affixed using an Araldite adhesive epoxy. Tensile tests were performed using a universal tensile testing machine (UTM Instron 5969; Instron, USA) equipped with a 50 KN load cell, while strain evolution was recorded by using digital image correlation (DIC; GOM Correlate, Germany). Similarly, the multifunctional CF-based strip composite lamina impregnated with SPE was analyzed by using a similar specimen preparation and testing scheme. The experiments were conducted in the tensile direction along the fibers. For each test, 3−5 specimens were examined, with a strain rate of 0.5 mm/min to capture and analyze the evolution of damage comprehensively. All tests are conducted on pristine uncycled specimens.

2.5.4. Interfacial Shear Strength (IFSS). The interfacial interaction between the CF and the SPE, as well as the effect of electrolyte percentage in the SPE, has been discussed in only a few papers,[49,50] despite its significant influence on the system's multifunctionality. Thus, in this work, the interfacial shear strength (IFSS) between the CF's surface and the SPE was assessed using a single fiber microdroplet shearing test. A microdroplet of the polymer (embedded length: ∼80 to ∼160 μm) was deposited onto the carbon fiber surface using a needle tip. The shape of the droplets and the contact angle (CA) of single-fiber microdroplets were recorded by OM to assess the impact of SPE on the wettability of the CFs. Subsequently, the droplets were cured following the designated cure cycle, and the final dimensions were evaluated for the interfacial test. Interfacial debonding of the droplet was initiated by a micrometer knife edge at a cross-head speed of 0.1 mm/min, utilizing a UTM Instron 5969 (Instron, USA) with a 5 N load cell. To determine the IFSS, the force−displacement curves and droplets' geometry were analyzed and utilized according to eq 8

$$\sigma = \frac{F}{\pi D l} \tag{8}$$

where F the maximum force, D is the fiber diameter, and l is the embedded length. The CA analysis was conducted by ImageJ, U.S. National Institutes of Health, 2022. Each respective CF/SPE formulation had a coefficient of variation (CV) of ≤15%. The experimental setup, IFSS schematic representation, and specimen preparation are listed in Figure 3.

3. RESULTS AND DISCUSSION

3.1. Solid Polymer Electrolyte (SPE). *3.1.1. Cure Kinetics Informed Fabrication of Epoxy-Based SPE.* For multifunctional structural batteries, the solid-state electrolyte is

https://doi.org/10.1021/acsami.4c08698
ACS Appl. Mater. Interfaces 2024, 16, 59128−59142

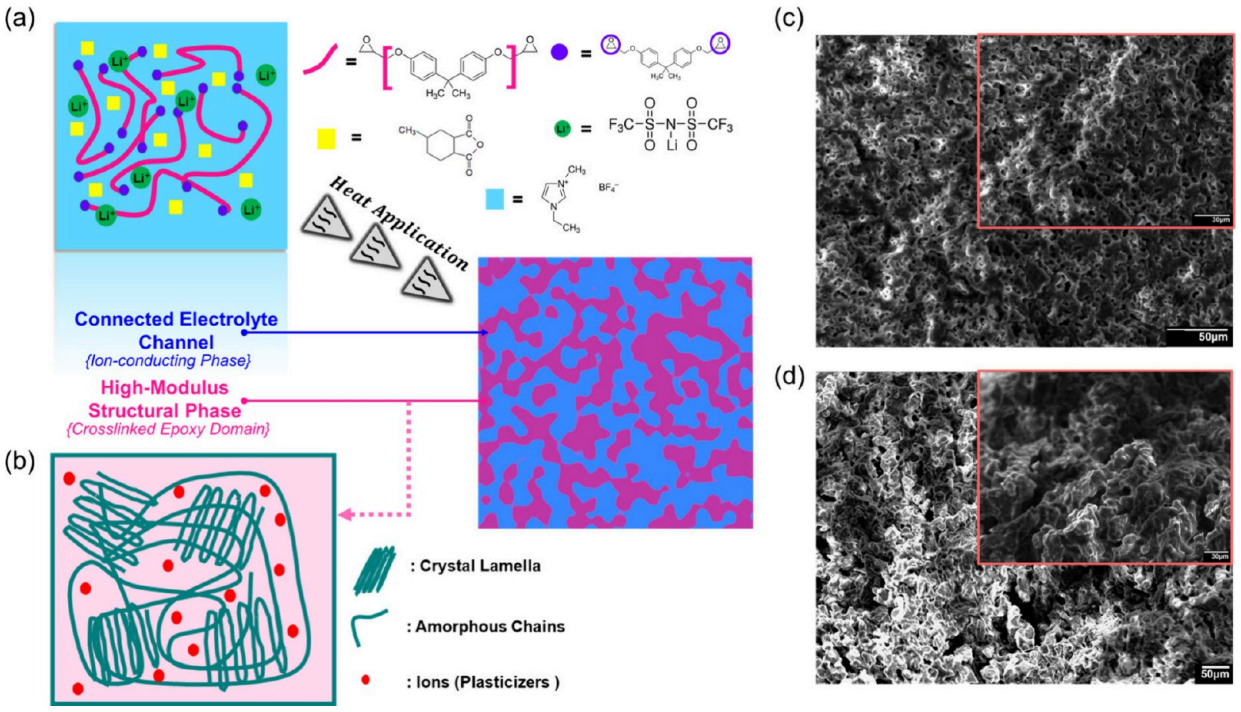

Figure 4. (a) Process of thermally initiated microphase separation. (b) Schematic of ions incorporated inside epoxy-rich domain acting as plasticizers. SEM images of the SPE microstructure post electrolyte extraction with zoom-in insets for (c) SPE 30 and (d) SPE 50.

a detrimental factor, as the bulk material must sustain a 3D connected domain to allow load bearing and ion conduction simultaneously, while successfully impregnating the CF electrodes. The 3D connected biphasic SPE with the constituents' chemical structure is schematically shown in Figure 4a. The phase-segregation procedure upon thermal initiation is outlined, showing a 2D cross-sectional schematic. Some ions from the polymerization-induced microphase separation (PIMS) electrolyte-rich domain can be incorporated into the epoxy-rich domain which act as plasticizers, thus increasing the free volume between polymer chains and increasing the chain's flexibility, as illustrated in Figure 4b. The SPE microstructural morphology is illustrated in Figure 4c,d and Figure S4.

The autocatalytic model was used to validate the impact of the applied cure cycle on the achieved conversion rate, as depicted in Figure 5. The temperature dependence of the SPE's reaction rate constants follows a typical relationship similar to the cross-linking of epoxy polymer. For instance, as the curing temperature increases, the respective reaction rate constant substantially increases due to the exponential relation predicted by the Arrhenius equation (eq 5). Once the reaction rate constants for each SPE formulation were identified, the activation energy and associated pre-exponential factor were obtained by analyzing the slope and intercept of the plot ln k_i against $1/T$, as illustrated in Figure 5a. After the autocatalytic reaction model was validated for each formulation and the kinetic parameters were obtained, it was evaluated by fitting the reaction rate as a function of DOC for various temperatures using eq 4. This analysis demonstrated a good fit for the experimental reaction rate, as shown in Figure 5b. The activation energy in Figure 5c elucidates the reaction mechanism in SPE, as one possibility of the lower activation energy at the latter stage (E_2) as the electrolyte % is increased is the additional role of IL as a catalyst,[51−53] providing new reaction pathways and lowering the required activation energy compared to the structural phase. Thus, the reaction rate is increased as reducing the required activation energy allows more reactant molecules to collide with enough energy to surmount the smaller energy barrier. With regard to E_1, in the case of SPE0, the energy required for the initial stage of curing E_1 is lower, i.e., the lower energy needed to surpass the barrier for the reaction to proceed. As electrolyte is introduced, the activation energy increases due to the suppression of the polymer chains and molecules movement (i.e., plasticizer effect). Therefore, the minimum energy that molecules must be moving for a collision to result in a chemical reaction, i.e., the activation energy increases. The effect of the electrolyte on the curing reaction in various SPEs is analyzed in Figure 5d,e showing the faster reaction rate and cross-linking evolution of SPE respectively as electrolyte content is increased. Based on the aforementioned analysis, a validated cure cycle was designed (Figure S5) to maximize the cross-linking, while also considering that polymerization and electrolyte entrapment can occur before premature macrophase separation, thus allowing for the adequate impregnation of the polymer between the carbon fibers before solidification.

3.1.2. Glass Transition Temperature (T_g). The influence of the electrolyte phase on the cross-linking state, crystallinity, and glass transition temperature (T_g) was investigated using calorimetry. The T_g exhibited a trend consistent with previous literature, showing a decrease upon the introduction of the electrolyte (Figure 6a and Figure S6). This decrease suggests a reduction in crystallinity and an increase in chain mobility, attributed to the plasticizer effect of the electrolyte. In Figure 6b, the Goron−Taylor equation for predicting polymer mixtures' T_g shows a good fit with a factor of less than unity, suggesting a phase-segregated polymer, opposed to a partitioned one,[54,55] thus implying favorable intermolecular interactions between the components.[56] It is worth noting that

https://doi.org/10.1021/acsami.4c08698
ACS Appl. Mater. Interfaces 2024, 16, 59128−59142

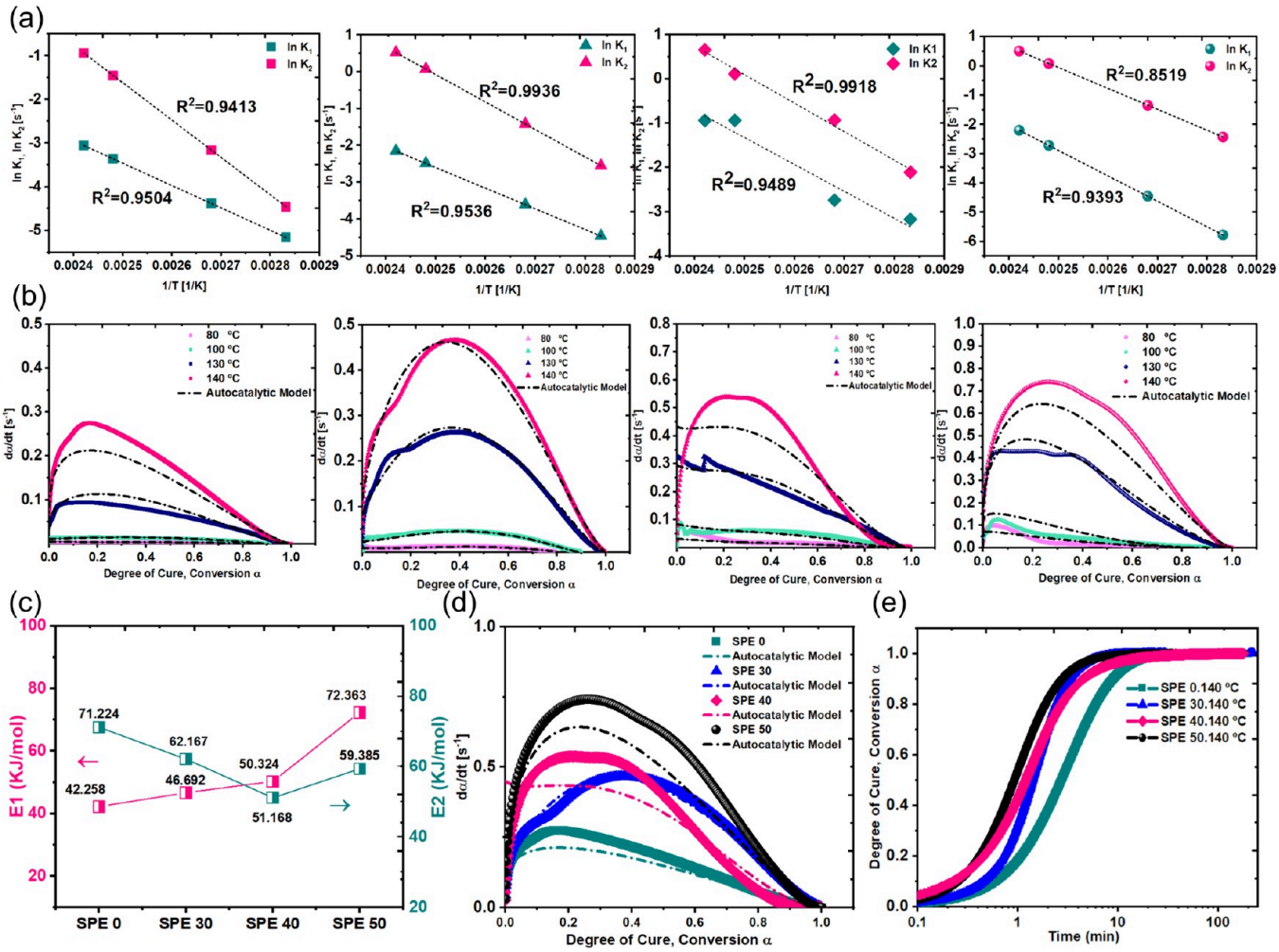

Figure 5. Cure kinetics results of SPE. (a) From left to right (SPE0, SPE30, SPE40, and SPE50) the reaction rate constants as derived by the Arrhenius equation. (b) From left to right (SPE0, SPE30, SPE40, and SPE50) the reaction rate $d\alpha/dt$ as a function of degree of cure (DOC) for isothermal experiments and autocatalytic model data. (c) Activation energy for different SPE formulations derived by Arrhenius equation fitting. (d) A comparison of the reaction rate for different SPE formulations as a function of the conversion degree at 140 °C. (e) Comparison of the DOC evolution for different SPE formulations as a function of time at 140 °C.

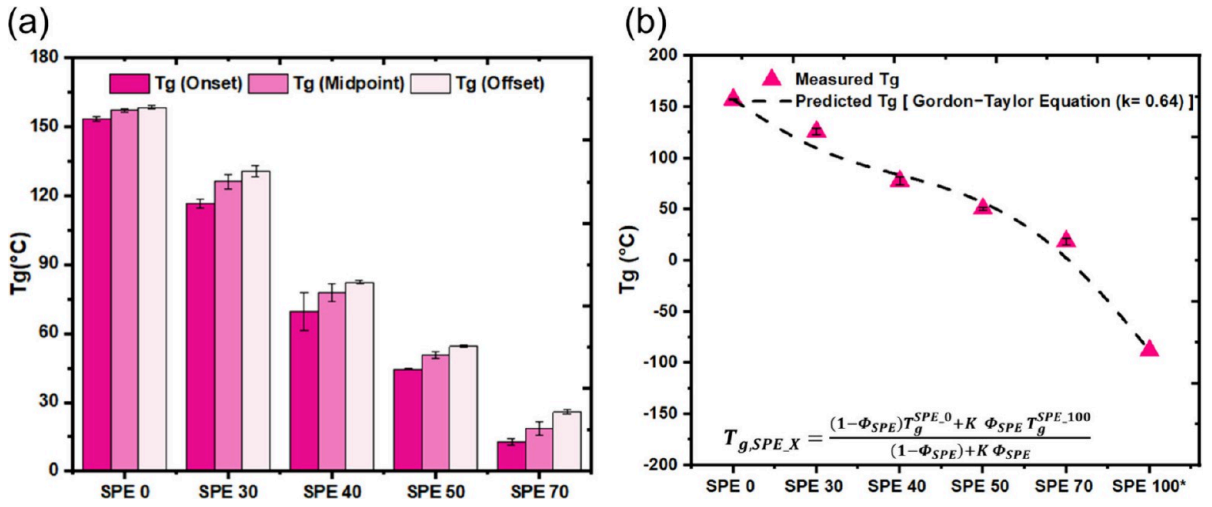

Figure 6. (a) Glass transition temperature of the SPE measured by DSC. (b) Measured T_g, midpoint, and prediction by the Gordon−Taylor equation.

formulations with a low T_g, such as SPE 70, may not be suitable for normal operating conditions of structural batteries. This underscores the importance of studying the thermal behavior of the SPE in the development of structural batteries.

https://doi.org/10.1021/acsami.4c08698
ACS Appl. Mater. Interfaces 2024, 16, 59128−59142

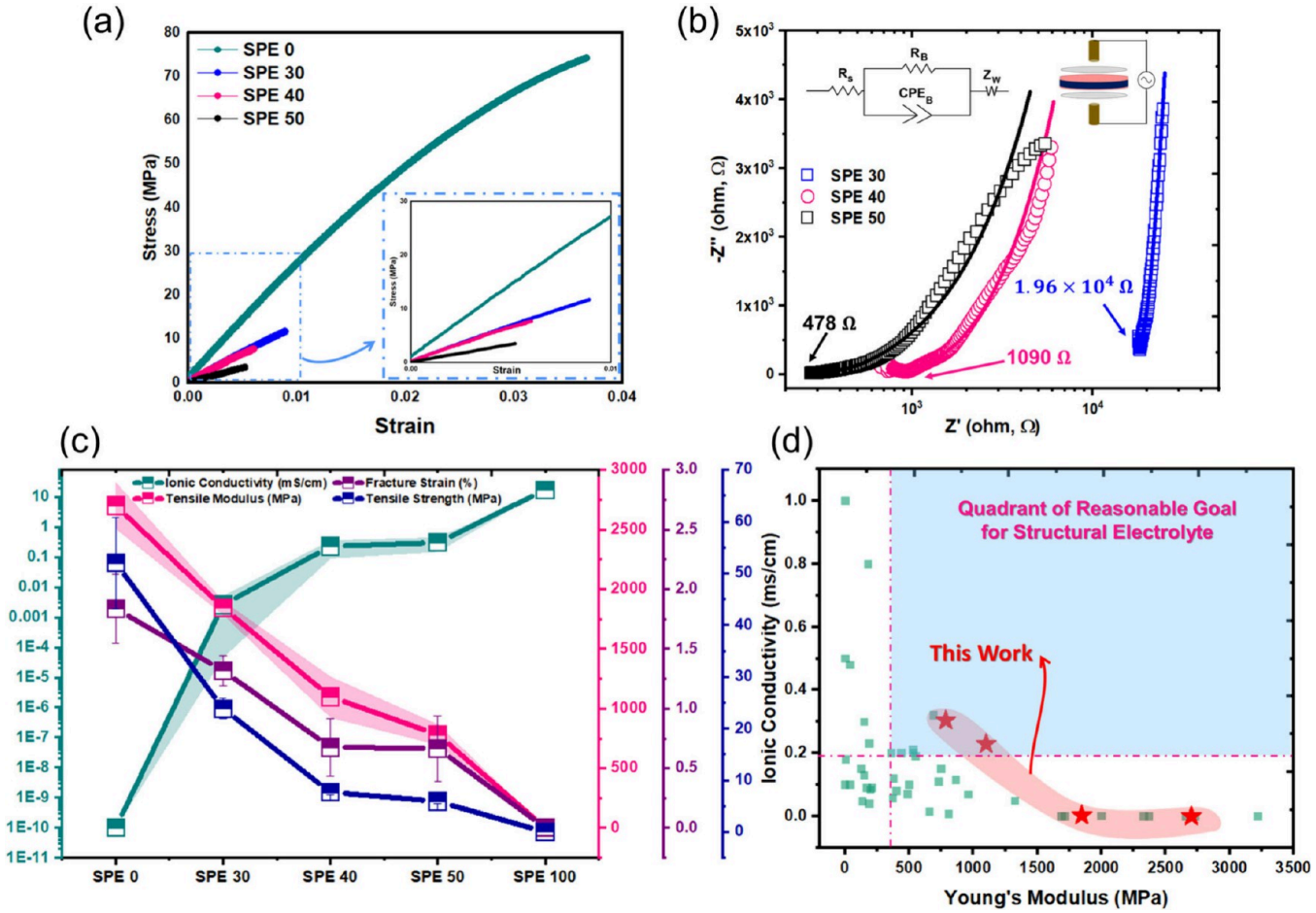

Figure 7. (a) Stress−strain curves of the SPEs from the tensile test. (b) Nyquist plot of the SPE for evaluating the ionic conductivity; the insets show the equivalent electrical circuit and the sample's schematic. (c) Mechano-electrochemical multifunctional plot comparing the ionic conductivity with tensile modulus, strength, and fracture strain. (d) Comparison of the multifunctional performance with previously reported SPEs; the detailed references are summarized in Table S1.

3.1.3. Multifunctional Analysis: Young's Modulus and Ionic Conductivity. The multifunctional performance of the SPE is shown in Figure 7. In contrast to the thin-film flexibility, the bulk SPE shows a more brittle behavior upon electrolyte addition, which can be attributed to the different microstructural morphology, as the frequent 3D bulk electrolyte domains have more adverse effects on the mechanical properties of SPE compared to the thin-film configuration. It is observed that further increasing the electrolyte content significantly drops the mechanical performance as shown in the stress−strain curves (Figure 7a). The ionic conductivity of the polymer was evaluated from the Nyquist plot obtained from EIS analysis; as shown in Figure 7b, the disappearance of the high-frequency semicircle reveals that total conductivity is mainly due to the lithium ion (i.e., low resistance of the electrode/sample interface). Furthermore, the inset exhibits the fitting of the equivalent electrical circuit, illustrating a parallel combination of bulk resistance and bulk capacitance. This arrangement can be driven by the ion's migration and the immobile polymer chains. Moreover, the appearance of a spike in the low-frequency range is indicative of Warburg impedance, reflecting an ion-diffusion-limited process.[57−59]

In Figure 7c, the mechano-electrochemical multifunctionality trade-off relation in the SPE is depicted. The increased ionic conductivity is accompanied by mechanical deterioration, especially the polymer's strength and fracture strain, showing a steep drop at around 145% and 95%, respectively, for only 30 wt % of electrolyte. Nevertheless, the achieved strength and mechano-electrochemical multifunctionality of the polymer were on par with and superior to previously presented SPEs. It is worth restating that no fillers or additives were introduced in this work, emphasizing the paramount effect of cure kinetics on SPE cross-linking formation and performance (Figure 7d, Table S1, and Figure S7). The reasonable goal of structural electrolytes is based on achieving within 1 order of magnitude of mechanical stiffness and ion conductivity of the constituents.[36,60,61]

3.2. CF-Based Multifunctional Lamina. *3.2.1. Multifunctional Lamina Fabrication.* To validate the concept that VACM can yield a higher packing fiber arrangement with superior mechanical performance lamina and minimal void, it is compared to another manufacturing method, vacuum bag only (VBO), using a commercial epoxy matrix. In Figure 8a, the effect of pressure on the thickness uniformity and fiber packing is discussed; VACM yielded around 15 μm thinner specimens than VBO with more uniform thickness, smaller standard deviation, and a frequent hexagonal array of fibers, which is the optimal fiber packing as shown in (Figure 8b,c and Figure S8). To ensure that the extreme pressure does not barrel the fibers or change their shape, the effect of pressure on

https://doi.org/10.1021/acsami.4c08698
ACS Appl. Mater. Interfaces 2024, 16, 59128−59142

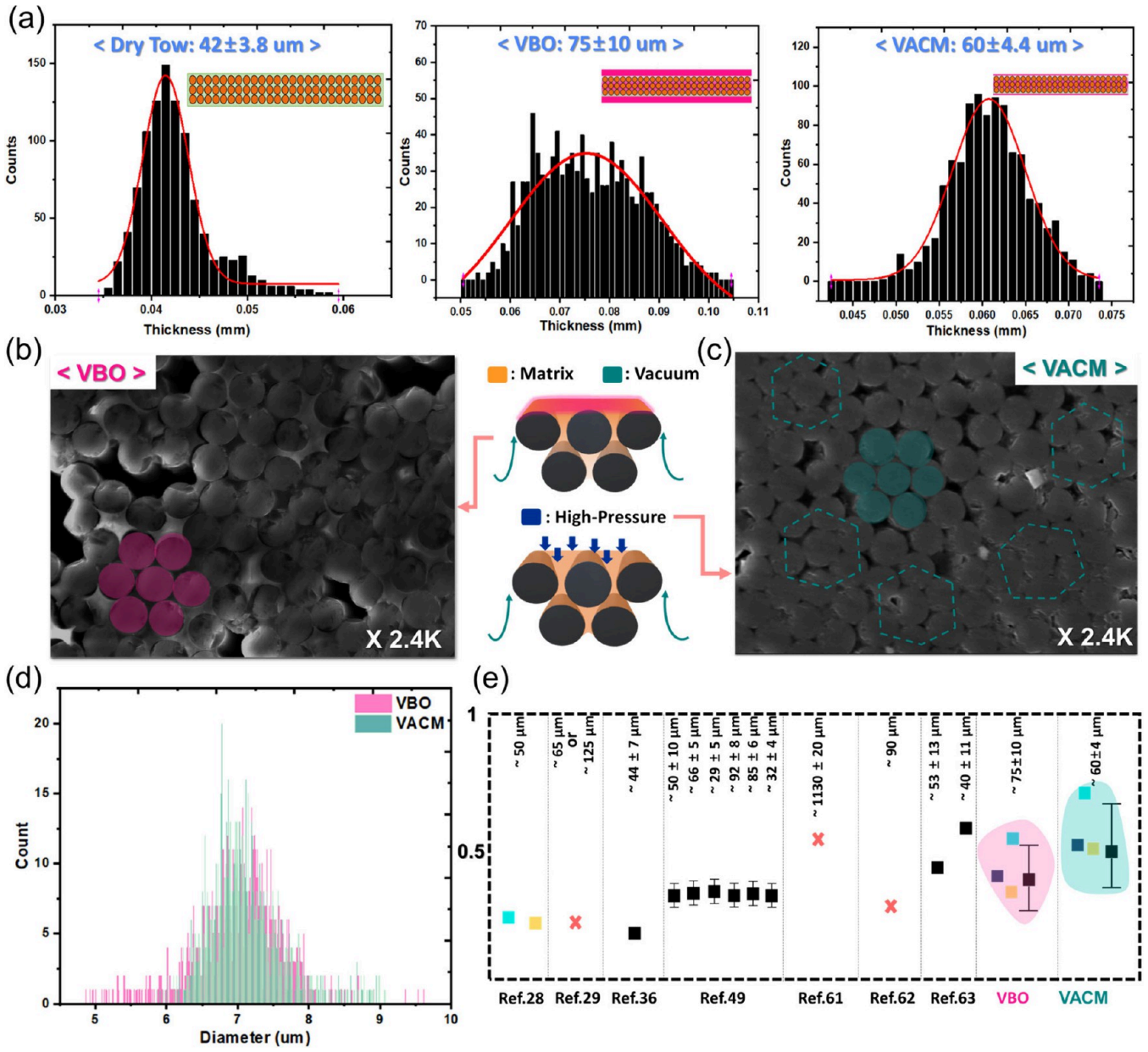

Figure 8. (a) Thickness distribution of dry, VBO, and VACM CFST-based specimens for ≥1000 measurements/each. Effect of the pressure on the fiber's arrangement and void frequency for (b) VBO and (c) VACM as depicted from SEM. (d) Fiber's diameters for both VBO and VACM. (e) Comparison of the obtained FVF with CF-based structural battery used in achieving ∼160% increase in FVF by VACM.[28,29,36,49,61−63] The measurements of FVF are based on ASTM D3171: blue, isostrain: gold, image processing: teal, theoretical maximum packing based on the apparent dimensions: black: not specified: rose, cross mark. More information on this work can be found in Figure S8.

the fiber's diameters is shown in Figure 8d. Using image processing, VACM and VBO fibers had an average diameter of 7.10 ± 0.51 and 7.06 ± 0.59 μm, respectively, which aligns closely with the manufacturer's reported data of 7 μm. This ultrathin, uniform, and low-void (Figure S9) robust design can be attributed to the fact that VACM can limit "flow-induced" voids, resulting from insufficient impregnation of fibers before resin gelation (Figure S10), offering superior mechanical advantages. Compared to some literature exploring single-ply CF-based structural batteries working as a negative electrode, the achieved fiber volume fraction (FVF) showed around a 160% increase, as shown in Figure 8e. The fiber volume fraction (FVF) results were validated through a rigorous combination of analytical (≥1000 measurements), experimental, and image processing methods. This comprehensive cross-validation approach is crucial for ensuring the accuracy and reliability of FVF measurements in thin single CF plies. Moreover, the achieved thickness of the lamina is also reported in Figure 8e, showing that FVF can be increased to approximately 57% at the expense of substantially increasing the lamina to an order of mm.[61] It is important to note that a theoretical comparison method is widely used in the literature to approximate the FVF based on the greatly varying dimensions of the lamina (i.e., black box in Figure 8e). In that regard, researchers report a theoretical FVF of 58% for an approximate thickness of 40 μm,[63] while the reported VACM can reach up to 66%. The statistical measurement and distribution of the thickness in Figure 8a highlight the

https://doi.org/10.1021/acsami.4c08698
ACS Appl. Mater. Interfaces 2024, 16, 59128−59142

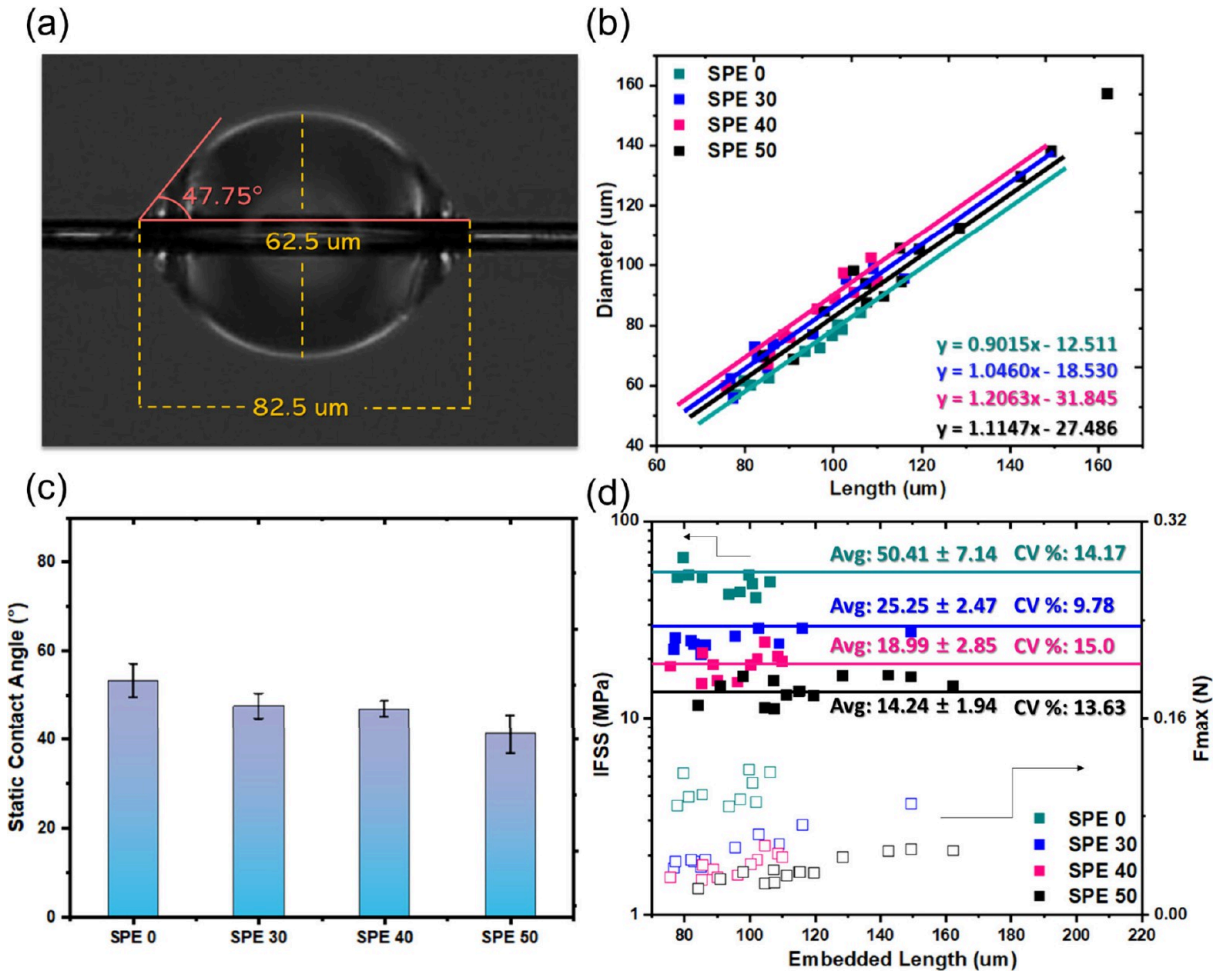

Figure 9. (a) SPE 30 microdroplet showing the geometry and the contact angle depicted from OM and ImageJ software. (b) Distribution of the microdroplets' length and diameter for various SPE formulations. (c) Static contact angle measurement of a single drop-on-fiber system. (d) Average IFSS and maximum force with respect to embedded length presented with a coefficient of variation (CV) of ≤15%.

importance of a large data set for statistical reliability, as ensuring validated and accurate FVF measurements is essential for the development and optimization of high-performance composite materials, as it directly impacts the material properties and performance of structural batteries. The integration of these various methods mitigates the limitations inherent in each approach, enhancing the overall measurement accuracy and robustness.

Such a configuration demonstrates significant structural potential, ensuring an ultralightweight structure with straight, uniform, evenly distributed, optimally packed, and low-void fibers. Furthermore, it provides a larger contact area between active materials (i.e., anode/cathode) with reduced separation distance, shortening the intercalation/conduction distance and thus offering electrochemical benefits as well.

3.2.2. Interfacial Shear Strength (IFSS). A sample of the SPE microdroplet is illustrated in Figure 9a, showcasing the droplet's geometry as analyzed by OM and ImageJ software. All droplets exhibited Carroll-shaped morphology, indicating a positive correlation between the droplet's diameter and embedded length. This relationship is depicted in Figure 9b, where all data points align along the diagonal for different SPE formulations, suggesting that the static contact angle is not highly dependent on the volume.[64] This observation is further supported by Figure 9c, which shows improved wettability as the electrolyte wt % is increased, leading to a slightly lower contact angle. The presence of the electrolyte flattens the droplet and spreads it on the fiber surface, implying a homogeneous mixture within the SPE.

The interfacial shear strength was evaluated based on the load−displacement debonding curve (Figure S11) and the dimensions of the CF/droplet. The interfacial adhesion strength demonstrates a notable decrease, as the IFSS decreases significantly upon successive introduction of electrolyte content. Specifically, for SPE 30, SPE 40, and SPE 50, the reduction in bond strength compared to SPE 0 corresponds to approximately 66.5%, 90.5%, and 111.9%, respectively, as illustrated in Figure 9d.

3.3. Multifunctional Battery Assembly. *3.3.1. Thermal Stability and Flammability of Hybrid Electrolyte Mixtures.* The thermal stability of the mixture, 1 M LiTFSI EC:DME (1:1v)- and 1 M LiTFSI IL-based electrolyte (herein named CE and IL, respectively), exhibited higher thermal stability than conventional electrolytes such as 1 M $LiPF_6$ in EC:DMC:EMC. The thermal stability and compatibility of the hybrid electrolyte, i.e., carbonate-based and ionic liquid-based systems, were evaluated by DSC for different volumetric ratios. The higher the percentage of the IL-based electrolyte in the mixture, the higher the thermal stability, as depicted in Figure 10. This can be attributed to the high thermal stability

https://doi.org/10.1021/acsami.4c08698
ACS Appl. Mater. Interfaces 2024, 16, 59128−59142

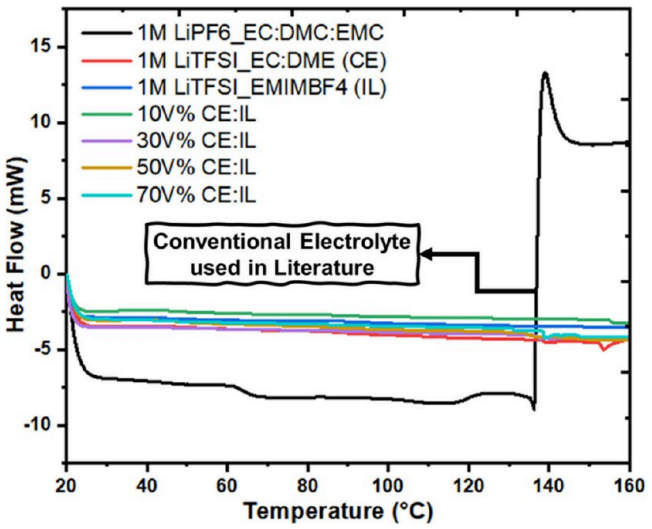

Figure 10. Electrolyte mixture thermal stability and compatibility via DSC.

of IL and the higher LiTFSI concentration,[65] making it a safer alternative to $LiPF_6$, which was commonly used in previous structural battery literature. Although this electrolyte possesses high ionic conductivity and transference number, it is volatile at elevated temperatures, as it can decompose and release various volatile gases such as C_2H_2, CH_4, CO, and CO_2, potentially leading to an explosion (i.e., rapid exothermic peak).

Furthermore, torching flammability tests were conducted for the same mixtures, and the results indicate that the intensity of combustion of the conventional electrolyte is much higher than that of the other mixtures. The burning and thermograms of the electrolyte mixtures (Movie S1) illustrate a noticeable contrast between the conventional electrolyte and the one utilized in this study, demonstrating much greater thermal stability, lower burning temperatures, and shorter self-extinguishing times.

3.3.2. Multifunctional Performance: Galvanostatic Charge/Discharge and Lamina Tensile Test. A galvanostatic cycling test and a lamina's tensile test were conducted as a proof-of-concept for assessing the CF lamina's ability to function as an integrated anode, current collector, and structural element. Figure 11a schematically illustrates the layered electrolyte domains (i.e., CE and SPE channels) facilitating ion conduction, while the closely packed CF structure enhances not only mechanical properties but also electronic conduction. Numerous morphological factors influence ionic and electronic conduction within batteries, including ionic resistance within the bulk electrolyte, resistance within polymer chains, diffusion within active materials, resistance within carbon fibers, and interface resistance at current connectors. The coating/impregnation of the electrolyte phase within the SPE was validated by checking the EDS elemental mapping for different CFST/SPE surfaces (Figure S12).

The discharge capacity, charging capacity, and Coulombic efficiency at different rated capacities of 0.1, 0.2, 0.5, 1, and 0.1 C are estimated for CFST-based battery, as well as SPE-impregnated CFST battery with SPE *X* (i.e., *X* = 30%, 40%, and 50%), as shown in Figure 11b,c,d. As noticed, SPE 50 exhibits relatively better capacity performance compared to SPE 40 and SPE 30, suggesting that a higher electrolyte percentage leads to enhanced performance. This can be attributed to the increased presence of the electrolyte phase, providing more routes for lithium ions to diffuse through active materials. Notably, if designed appropriately, a higher electrolyte percentage can lead to polymer chains possessing greater mobility and flexibility, potentially facilitating ion conduction through chain hopping mechanisms.

However, it is worth noting that for all cells, the initial cycles showed steep deterioration, which could negatively impact overall performance. The formation protocol, although not discussed or optimized for structural batteries, holds immense significance for stability and solid electrolyte interphase (SEI) formation.[65−67] Nevertheless, the consistently high Coulombic efficiency (CE) shown in Figure 11d underscores minimal electron loss, even at 0.5 C, instilling confidence in the potential commercialization of structural batteries. The rate performance study of different SPE formulations in Figure 11b−d demonstrates that upon varying the *C*-rate, the capacity returns to its approximate initial value, showing the reversibility and stability of the cycling. Moreover, the capacity and potential curves presented in Figure S13a represent how the voltage profiles change as the cells' discharge/charge, similar to relevant CF-based battery literature.[28,29,36,61,62]

Moreover, Figure 11e depicts the CCCV galvanostatic charge and discharge (GCD) profile of a fresh SPE 40 cell at 10.4 mA g^{-1}, operating continuously for over 1250 h, corresponding to more than 250 cycles as illustrated in Figure 11f and Figure S13b, in which both SPE 40 and SPE 50 are cycled for a long period at 25 0 ± 0.3 °C to check the cells' stability. Despite the Coulombic efficiency averaging over 99.98% due to the reversibility of the reaction, the rated capacity deteriorates notably, particularly in the initial cycles. This can also be observed in the initial cycles during the rate performance study. Hence, future advancements in structural battery technology must prioritize the development of specialized formation and conditioning precycling protocols to ensure the stable formation of SEI layer on the CF anode and ensure the reversible lithium delithiation/lithiation. In spite of that, the results presented in this study show synonymous behavior to a recent study employing graphite on woven fabric as the anode.[1] The elastic Young modulus was assessed through a tensile test, with strain evolution recorded via in situ digital image correlation (DIC) (Figure S14). Undoubtedly, the optimized packing informed by cure kinetics, which facilitated enhanced cross-linking and impregnation, contributed to the overall multifunctionality, particularly in terms of mechanical stiffness. Many fabrication factors such as carbon fiber types, structural phase, electrolyte phase, electrolyte content, cell configuration, mechanical modulus, discharge capacity at different *C*-rates, and first-cycle discharge capacity can dictate the performance of the CF structural battery, which make making comparisons very challenging. On that regard, a comprehensive comparison table is presented for CF-based anode material in the scope of structural battery in Table S2. This analysis underscores how such a design methodology holds the potential to advance the adoption of smart functional composites, promoting increased efficiency and sustainability in the near future.

4. CONCLUSIONS

Through this work, we have successfully developed an epoxy-based solid polymer electrolyte (SPE) with unprecedented

https://doi.org/10.1021/acsami.4c08698
ACS Appl. Mater. Interfaces 2024, 16, 59128−59142

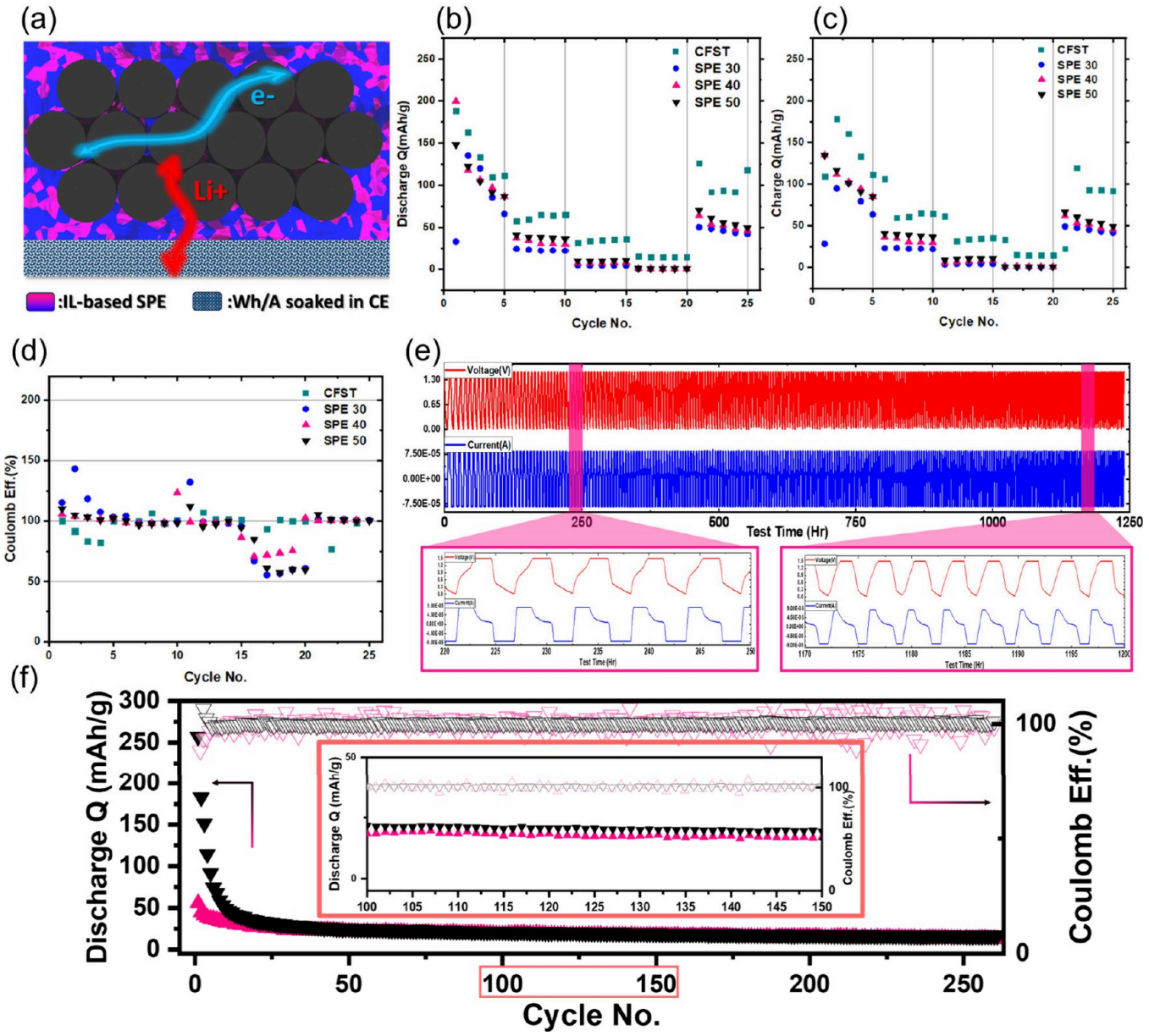

Figure 11. (a) Schematic of ionic and electronic conductions in CF/SPE-based multifunctional lamina. Rate performance of different CFST/SPE-based formulations. (b) Specific discharge capacity. (c) Specific charge capacity. (d) Coulombic efficiency. (e) CCCV galvanostatic charge and discharge (GCD) profile of CFST|SPE 40 at 10.4 mA g^{-1}. (f) Cycling stabilities of CFST|SPE 40 (pink) and CFST|SPE 50 (black) at 10.4 mA g^{-1}.

performance, informed by cure kinetics, and incorporated a plasticizing and ionically conductive ionic liquid, along with a weak-binding lithium salt, through a single-pot thermally initiated microphase separation. This approach enabled facile fabrication, leading to a forefront multifunctional performance without the need for additives or fillers. A multifunctional SPE-impregnated CF lamina was fabricated using robust vacuum-assisted compression molding, exhibiting superior morphology, low voids, and optimal CF packing, thereby potentially enhancing the structural, electronic, and electrochemical performance.

As a proof-of-concept, a multifunctional lamina was integrated into a coin-cell battery with a hybrid electrolyte system, and its performance was evaluated. Structurally, the ultrathin multifunctional lamina demonstrated superior performance with a modulus higher than conventional structural elements ($E \approx 120$ GPa). However, while the cycling stability showed consistent performance for over 1250 h, the discharge capacity needs improvement, especially through optimization of the preconditioning formation protocol to achieve stable and efficient solid electrolyte interphase (SEI) growth and protect structural batteries from initial rapid capacity deterioration.

In conclusion, this study provides valuable insights into the development of an ultrathin structural lamina with stiffness comparable to conventional elements, offering promising solutions for sustainable next-generation multifunctional energy storage applications. Future work will focus on further improving SPE properties, addressing the structural/electrochemical trade-off, and leveraging the superior properties of the epoxy-based SPE to advance lithium metal batteries by effectively suppressing lithium dendrite growth.[68,69]

https://doi.org/10.1021/acsami.4c08698
ACS Appl. Mater. Interfaces 2024, 16, 59128−59142

■ ASSOCIATED CONTENT

Data Availability Statement

The data that support the findings of this study are available from the corresponding author upon request.

Supporting Information

The Supporting Information is available free of charge at https://pubs.acs.org/doi/10.1021/acsami.4c08698.

CF-based electrode preparation; cure kinetics analysis of SPE; stochastic analysis of CFST morphology; SEM images of the SPE microstructure after the electrolyte extraction; effect of cure cycle on the evolution of degree of cure (DOC); DSC thermal analysis of different SPE formulations; significance of SPE cure kinetics analysis on the multifunctional performance; methods to measure FVF; single layer void analysis; void migration and transport in VBO/VACM processes; load−displacement curves of IFSS test; EDS mapping analysis of CFST/SPE surface; typical discharge profiles of different CF/SPE cells; comparison of fabrication specifications and properties of CF-based structural battery negative electrodes; and tensile curves of the CF/SPE electrode lamina with Young's modulus (PDF)

Hybrid electrolyte flammability test (Movie S1) (MP4)

■ AUTHOR INFORMATION

Corresponding Author

Seong Su Kim − *Department of Mechanical Engineering, Korea Advanced Institute of Science & Technology (KAIST), Daejeon 305-701, Republic of Korea;* orcid.org/0000-0001-8722-0505; Phone: +82-42-350-3018; Email: seongsukim@kaist.ac.kr

Authors

Mohamad A. Raja − *Department of Mechanical Engineering, Korea Advanced Institute of Science & Technology (KAIST), Daejeon 305-701, Republic of Korea;* orcid.org/0009-0007-4646-9751

Su Hyun Lim − *Department of Mechanical Engineering, Korea Advanced Institute of Science & Technology (KAIST), Daejeon 305-701, Republic of Korea*

Doyun Jeon − *Department of Aerospace Engineering, Korea Advanced Institute of Science & Technology (KAIST), Daejeon 305-701, Republic of Korea*

Sangyoon Bae − *Department of Mechanical Engineering, Korea Advanced Institute of Science & Technology (KAIST), Daejeon 305-701, Republic of Korea*

Woong Oh − *Department of Mechanical Engineering, Korea Advanced Institute of Science & Technology (KAIST), Daejeon 305-701, Republic of Korea*

Inyeong Yang − *Department of Mechanical Engineering, Korea Advanced Institute of Science & Technology (KAIST), Daejeon 305-701, Republic of Korea*

Dajeong Kang − *Department of Mechanical Engineering, Korea Advanced Institute of Science & Technology (KAIST), Daejeon 305-701, Republic of Korea*

Jawon Ha − *Department of Mechanical Engineering, Korea Advanced Institute of Science & Technology (KAIST), Daejeon 305-701, Republic of Korea*

Ha Eun Lee − *Department of Mechanical Engineering, Korea Advanced Institute of Science & Technology (KAIST), Daejeon 305-701, Republic of Korea*

Il-Kwon Oh − *Department of Mechanical Engineering, Korea Advanced Institute of Science & Technology (KAIST), Daejeon 305-701, Republic of Korea;* orcid.org/0000-0002-6705-7664

Sanha Kim − *Department of Mechanical Engineering, Korea Advanced Institute of Science & Technology (KAIST), Daejeon 305-701, Republic of Korea;* orcid.org/0000-0002-3548-6173

Complete contact information is available at: https://pubs.acs.org/10.1021/acsami.4c08698

Author Contributions

M.A.R.: conceptualization, methodology, data curation, investigation, visualization, validation, writing−original draft, writing−reviewing and editing; S.H.L.: methodology, writing−reviewing and editing; D.J.: methodology, visualization; S.B.: methodology, data curation; W.O.: methodology; I.Y.: investigation; D.K.: methodology; J.H.: methodology; H.E.L.: investigation; I.K.O.: supervision; S.K.: supervision; S.S.K.: supervision, writing−reviewing and editing.

Notes

The authors declare no competing financial interest.

■ ACKNOWLEDGMENTS

This work was supported by the National Research Foundation of Korea (NRF) grant funded by the Korea government (MSIT) (No. 2020R1A2C201096512) and by the National R&D Program through the National Research Foundation of Korea (NRF) funded by Ministry of Science and ICT (RS-2023-00260461).

■ REFERENCES

(1) Han, Z.; Zhu, J.; Feng, Y.; Zhang, W.; Xiong, Y.; Zhang, W. Manufacturing Carbon Fabric Composite Structural Batteries Using Spray with High-Pressure and High-Temperature and Vacuum-Bag Assisted Infusion Techniques. *Compos. Sci. Technol.* **2024**, *245*, No. 110321.

(2) Pyo, J.; Park, H.-W.; Jang, M.-S.; Choi, J.-S.; Kumar, S. K. S.; Kim, C.-G. Tubular Laminated Composite Structural Battery. *Compos. Sci. Technol.* **2021**, *208*, No. 108646.

(3) Zhou, H.; Li, H.; Li, L.; Liu, T.; Chen, G.; Zhu, Y.; Zhou, L.; Huang, H. Structural Composite Energy Storage Devices-A Review. *Materials Today Energy* **2022**, *24*, No. 100924.

(4) Asp, L. E.; Johansson, M.; Lindbergh, G.; Xu, J.; Zenkert, D. Structural Battery Composites: A Review. *Functional Composites and Structures* **2019**, *1* (4), No. 042001.

(5) Zhou, Y.; Qi, H.; Yang, J.; Bo, Z.; Huang, F.; Islam, M. S.; Lu, X.; Dai, L.; Amal, R.; Wang, C. H.; Han, Z. Two-Birds-One-Stone: Multifunctional Supercapacitors Beyond Traditional Energy Storage. *Energy Environ. Sci.* **2021**, *14* (4), 1854−1896.

(6) Pradere, C.; Batsale, J. C.; Goyhénèche, J. M.; Pailler, R.; Dilhaire, S. Thermal Properties of Carbon Fibers at Very High Temperature. *Carbon* **2009**, *47*, 737−743.

(7) Zhao, Q.; Zhang, K.; Zhu, S.; Xu, H.; Cao, D.; Zhao, L.; Zhang, R.; Yin, W. Review on the Electrical Resistance/Conductivity of Carbon Fiber Reinforced Polymer. *Applied Sciences* **2019**, *9* (11), 2390.

(8) Gupta, A.; Dhakate, S. R.; Pal, P.; Dey, A.; Iyer, P. K.; Singh, D. K. Effect of Graphitization Temperature on Structure and Electrical Conductivity of Poly-Acrylonitrile Based Carbon Fibers. *Diamond Relat. Mater.* **2017**, *78*, 31−38.

(9) Wazeer, A.; Das, A.; Abeykoon, C.; Sinha, A.; Karmakar, A. Composites for Electric Vehicles and Automotive Sector: A Review. *Green Energy and Intelligent Transportation* **2023**, *2*, No. 100043.

(10) Parveez, B.; Kittur, M. I.; Badruddin, I. A.; Kamangar, S.; Hussien, M.; Umarfarooq, M. A. Scientific Advancements in Composite Materials for Aircraft Applications: A Review. *Polymers* **2022**, *14* (22), 5007.
(11) Sehar, B.; Waris, A.; Gilani, S. O.; Ansari, U.; Mushtaq, S.; Khan, N. B.; Jameel, M.; Khan, M. I.; Bafakeeh, O. T.; Tag-ElDin, E. S. M. The Impact of Laminations on the Mechanical Strength of Carbon-Fiber Composites for Prosthetic Foot Fabrication. *Crystals* **2022**, *12* (10), 1429.
(12) Islam, M. S.; Deng, Y.; Tong, L.; Faisal, S. N.; Roy, A. K.; Minett, A. I.; Gomes, V. G. Grafting Carbon Nanotubes Directly Onto Carbon Fibers for Superior Mechanical Stability: Towards Next Generation Aerospace Composites and Energy Storage Applications. *Carbon* **2016**, *96*, 701−710.
(13) Luo, H.; Lu, H.; Qiu, J. Carbon Fibers Surface-Grown with Helical Carbon Nanotubes and Polyaniline for High-Performance Electrode Materials and Flexible Supercapacitors. *J. Electroanal. Chem.* **2018**, *828*, 24−32.
(14) Subhani, K.; Jin, X.; Mahon, P. J.; Lau, A. K. T.; Salim, N. V. Graphene Aerogel Modified Carbon Fiber Reinforced Composite Structural Supercapacitors. *Compos. Commun.* **2021**, *24*, No. 100663.
(15) Deka, B. K.; Hazarika, A.; Kwon, O.; Kim, D.; Park, Y.-B.; Park, H. W. Multifunctional Enhancement of Woven Carbon Fiber/ZnO Nanotube-Based Structural Supercapacitor and Polyester Resin-Domain Solid-Polymer Electrolytes. *Chem. Eng. J.* **2017**, *325*, 672−680.
(16) Deka, B. K.; Hazarika, A.; Kim, J.; Kim, N.; Jeong, H. E.; Park, Y.-B.; Park, H. W. Bimetallic Copper Cobalt Selenide Nanowire-Anchored Woven Carbon Fiber-Based Structural Supercapacitors. *Chem. Eng. J.* **2019**, *355*, 551−559.
(17) Moyer, K.; Meng, C.; Marshall, B.; Assal, O.; Eaves, J.; Perez, D.; Karkkainen, R.; Roberson, L.; Pint, C. L. Carbon Fiber Reinforced Structural Lithium-Ion Battery Composite: Multifunctional Power Integration for CubeSats. *Energy Storage Materials* **2020**, *24*, 676−681.
(18) Choi, J.; Zabihi, O.; Ahmadi, M.; Naebe, M. Advancing Structural Batteries: Cost-Efficient High-Performance Carbon Fiber-Coated LiFePO4 Cathodes. *RSC Adv.* **2023**, *13* (44), 30633−30642.
(19) Jiang, Q.; Beutl, A.; Kühnelt, H.; Bismarck, A. Structural Composite Batteries Made From Carbon Fibre Reinforced Electrodes/Polymer Gel Electrolyte Prepregs. *Compos. Sci. Technol.* **2023**, *244*, No. 110312.
(20) Petrushenko, D.; Rahmati, Z.; Barazanchy, D.; De Backer, W.; Mustain, W. E.; White, R. E.; Ziehl, P.; Coman, P. T. Dip-Coating of Carbon Fibers for the Development of Lithium Iron Phosphate Electrodes for Structural Lithium-Ion Batteries. *Energy Fuels* **2023**, *37*, 711−723.
(21) Snyder, J. F.; Wong, E. L.; Hubbard, C. W. Evaluation of Commercially Available Carbon Fibers, Fabrics, and Papers for Potential Use in Multifunctional Energy Storage Applications. *J. Electrochem. Soc.* **2009**, *156*, A215.
(22) Kjell, M. H.; Jacques, E.; Zenkert, D.; Behm, M.; Lindbergh, G. PAN-Based Carbon Fiber Negative Electrodes for Structural Lithium-Ion Batteries. *J. Electrochem. Soc.* **2011**, *158*, A1455.
(23) Shundo, A.; Yamamoto, S.; Tanaka, K. Network Formation and Physical Properties of Epoxy Resins for Future Practical Applications. *JACS Au* **2022**, *2*, 1522−1542.
(24) Xu, H.; Zhang, X.; Yu, Y.; Yu, Y.; Yang, Z.; Zhu, X.; Weng, L. Enhancement of Mechanical Properties of Epoxy Resin Matrix Adhesives by High-Performance Fillers. *J. Polym. Res.* **2023**, *30*, 30.
(25) Wegmann, A. Chemical Resistance of Waterborne Epoxy/Amine Coatings. *Prog. Org. Coat.* **1997**, *32*, 231−239.
(26) Zheng, Y.; Yao, Y.; Ou, J.; Li, M.; Luo, D.; Dou, H.; Li, Z.; Amine, K.; Yu, A.; Chen, Z. A Review of Composite Solid-State Electrolytes for Lithium Batteries: Fundamentals, Key Materials and Advanced Structures. *Chem. Soc. Rev.* **2020**, *49* (23), 8790−8839.
(27) Zhou, D.; Shanmukaraj, D.; Tkacheva, A.; Armand, M.; Wang, G. Polymer Electrolytes for Lithium-Based Batteries: Advances and Prospects. *Chem.* **2019**, *5*, 2326−2352.
(28) Carlstedt, D.; Rittweger, F.; Runesson, K.; Navarro-Suárez, A. M.; Xu, J.; Duan, S.; Larsson, F.; Riemschneider, K.-R.; Asp, L. E. Experimental and Computational Characterization of Carbon Fibre Based Structural Battery Electrode Laminae. *Compos. Sci. Technol.* **2022**, *220*, No. 109283.
(29) Asp, L. E.; Bouton, K.; Carlstedt, D.; Duan, S.; Harnden, R.; Johannisson, W.; Johansen, M.; Johansson, M. K. G.; Lindbergh, G.; Liu, F.; et al. A Structural Battery and its Multifunctional Performance. *Advanced Energy and Sustainability Research* **2021**, *2*, No. 2000093.
(30) Hess, S.; Wohlfahrt-Mehrens, M.; Wachtler, M. Flammability of Li-Ion Battery Electrolytes: Flash Point and Self-Extinguishing Time Measurements. *J. Electrochem. Soc.* **2015**, *162*, A3084.
(31) Ran, Z.; Liu, X.; Jiang, X.; Wu, Y.; Liao, H. Study on Curing Kinetics of Epoxy-Amine to Reduce Temperature Caused by the Exothermic Reaction. *Thermochim. Acta* **2020**, *692*, No. 178735.
(32) Huang, F.; Zhou, Y.; Sha, Z.; Peng, S.; Chang, W.; Cheng, X.; Zhang, J.; Brown, S. A.; Han, Z.; Wang, C.-H. Surface Functionalization of Electrodes and Synthesis of Dual-Phase Solid Electrolytes for Structural Supercapacitors. *ACS Applied Materials Interfaces* **2022**, *14*, 30857−30871.
(33) Kwon, S. J.; Kim, T.; Jung, B. M.; Lee, S. B.; Choi, U. H. Multifunctional Epoxy-Based Solid Polymer Electrolytes for Solid-State Supercapacitors. *ACS Applied Materials Interfaces* **2018**, *10*, 35108−35117.
(34) Yu, Y.; Zhang, B.; Wang, Y.; Qi, G.; Tian, F.; Yang, J.; Wang, S. Co-continuous Structural Electrolytes Based on Ionic Liquid, Epoxy Resin and Organoclay: Effects of Organoclay Content. *Materials & Design* **2016**, *104*, 126−133.
(35) Huang, F.; Singer, G.; Zhou, Y.; Sha, Z.; Chen, J.; Han, Z.; Brown, S. A.; Zhang, J.; Wang, C. H. Creating Ionic Pathways in Solid-State Polymer Electrolyte by using PVA-Coated Carbon Nanofibers. *Compos. Sci. Technol.* **2021**, *207*, No. 108710.
(36) Johannisson, W.; Ihrner, N.; Zenkert, D.; Johansson, M.; Carlstedt, D.; Asp, L. E.; Sieland, F. Multifunctional Performance of a Carbon Fiber UD Lamina Electrode for Structural Batteries. *Compos. Sci. Technol.* **2018**, *168*, 81−87.
(37) Song, B. F.; Dhanabalan, A.; Biswal, S. L. Evaluating the Capacity Ratio and Prelithiation Strategies for Extending Cyclability in Porous Silicon Composite Anodes and Lithium Iron Phosphate Cathodes for High Capacity Lithium-Ion Batteries. *Journal of Energy Storage* **2020**, *28*, No. 101268.
(38) Yun, Y. S.; Kim, J. H.; Lee, S.-Y.; Shim, E.-G.; Kim, D.-W. Cycling Performance and Thermal Stability of Lithium Polymer Cells Assembled with Ionic Liquid-Containing Gel Polymer Electrolytes. *J. Power Sources* **2011**, *196*, 6750−6755.
(39) Guerfi, A.; Dontigny, M.; Charest, P.; Petitclerc, M.; Lagace, M.; Vijh, A.; Zaghib, K. Improved Electrolytes for Li-Ion Batteries: Mixtures of Ionic Liquid and Organic Electrolyte with Enhanced Safety and Electrochemical Performance. *J. Power Sources* **2010**, *195*, 845−852.
(40) López, J.; Rico, M.; Montero, B.; Díez, J.; Ramírez, C. Polymer Blends Based on an Epoxy-Amine Thermoset and a Thermoplastic. *J. Therm. Anal. Calorim.* **2009**, *95*, 369−376.
(41) Ellis, B. *Chemistry and Technology of Epoxy Resins*; Springer: Netherlands, 1993, 72−116.
(42) Voto, G.; Sequeira, L.; Skordos, A. A. Formulation Based Predictive Cure Kinetics Modelling of Epoxy Resins. *Polymers* **2021**, *236*, 124304.
(43) Teil, H.; Page, S. A.; Michaud, V.; Månson, J.-A. E. TTT-Cure Diagram of an Anhydride-Cured Epoxy System Including Gelation, Vitrification, Curing Kinetics Model, and Monitoring of the Glass Transition Temperature. *J. Appl. Polym. Sci.* **2004**, *93*, 1774−1787.
(44) Garschke, C.; Parlevliet, P. P.; Weimer, C.; Fox, B. L. Cure Kinetics and Viscosity Modelling of a High-Performance Epoxy Resin Film. *Polym. Test.* **2013**, *32*, 150−157.
(45) Hardis, R.; Jessop, J. L. P.; Peters, F. E.; Kessler, M. R. Cure Kinetics Characterization and Monitoring of an Epoxy Resin using

https://doi.org/10.1021/acsami.4c08698
ACS Appl. Mater. Interfaces 2024, 16, 59128−59142

DSC, Raman Spectroscopy, and DEA. *Composites Part A: Applied Science and Manufacturing* **2013**, *49*, 100−108.
(46) Xu, H.; Tian, G.; Meng, Y.; Li, X.; Wu, D. Cure Kinetics of a Nadic Methyl Anhydride Cured Tertiary Epoxy Mixture. *Thermochim. Acta* **2021**, *701*, No. 178942.
(47) Weingarth, D.; Drumm, R.; Foelske-Schmitz, A.; Kötz, R.; Presser, V. An Electrochemical in situ Study of Freezing and Thawing of Ionic Liquids in Carbon Nanopores. *Phys. Chem. Chem. Phys.* **2014**, *16* (39), 21219−21224.
(48) International, A. *ASTM D638-14, Standard Test Method for Tensile Properties of Plastics*; ASTM International: 2015.
(49) Xu, J.; Johannisson, W.; Johansen, M.; Liu, F.; Zenkert, D.; Lindbergh, G.; Asp, L. E. Characterization of the Adhesive Properties Between Structural Battery Electrolytes and Carbon Fibers. *Compos. Sci. Technol.* **2020**, *188*, No. 107962.
(50) Raja, M. A.; Lim, S. H.; Jeon, D.; Hong, H.; Yang, I.; Kim, S.; Kim, S. S. An Investigation of Interfacial Strength in Epoxy-based Solid Polymer Electrolytes for Structural Composite Batteries. *Composites Research* **2023**, *36* (6), 416−421.
(51) Liu, L.; Gao, S.; Jiang, Z.; Zhang, Y.; Gui, D.; Zhang, S. Amide-Functionalized Ionic Liquids as Curing Agents for Epoxy Resin: Preparation, Characterization, and Curing Behaviors with TDE-85. *Industrial Engineering Chemistry Research* **2019**, *58*, 14088−14097.
(52) Orduna, L.; Razquin, I.; Aranburu, N.; Guerrica-Echevarría, G. Are Ionic Liquids Effective Curing Agents for Preparing Epoxy Adhesives? *Int. J. Adhes. Adhes.* **2023**, *125*, No. 103438.
(53) Mąka, H.; Spychaj, T.; Zenker, M. High Performance Epoxy Composites Cured with Ionic Liquids. *J. Ind. Eng. Chem.* **2015**, *31*, 192−198.
(54) Espíndola, S. P.; Norder, B.; Koper, G. J. M.; Picken, S. J. The Glass Transition Temperature of Heterogeneous Biopolymer Systems. *Biomacromolecules* **2023**, *24*, 1627−1637.
(55) Seo, M.; Hillmyer, M. A. Reticulated Nanoporous Polymers by Controlled Polymerization-Induced Microphase Separation. *Science* **2012**, *336*, 1422−1425.
(56) Kalogeras, I. M.; Brostow, W. Glass Transition Temperatures in Binary Polymer Blends. *J. Polym. Sci., Part B: Polym. Phys.* **2009**, *47*, 80−95.
(57) Arya, A.; Sadiq, M.; Sharma, A. L. Effect of Variation of Different Nanofillers on Structural, Electrical, Dielectric, and Transport Properties of Blend Polymer Nanocomposites. *Ionics* **2018**, *24*, 2295−2319.
(58) Liu, W.; Liu, N.; Sun, J.; Hsu, P.-C.; Li, Y.; Lee, H.-W.; Cui, Y. Ionic Conductivity Enhancement of Polymer Electrolytes with Ceramic Nanowire Fillers. *Nano Lett.* **2015**, *15*, 2740−2745.
(59) Liu, W.; Lin, D.; Sun, J.; Zhou, G.; Cui, Y. Improved Lithium Ionic Conductivity in Composite Polymer Electrolytes with Oxide-Ion Conducting Nanowires. *ACS Nano* **2016**, *10*, 11407−11413.
(60) Shirshova, N.; Bismarck, A.; Carreyette, S.; Fontana, Q. P. V.; Greenhalgh, E. S.; Jacobsson, P.; Johansson, P.; Marczewski, M. J.; Kalinka, G.; Kucernak, A. R. J.; et al. Structural Supercapacitor Electrolytes Based on Bicontinuous Ionic Liquid−Epoxy Resin Systems. *J. Mater. Chem. A* **2013**, *1* (48), 15300−15309.
(61) Yu, Y.; Zhang, B.; Feng, M.; Qi, G.; Tian, F.; Feng, Q.; Yang, J.; Wang, S. Multifunctional Structural Lithium Ion Batteries based on Carbon Fiber Reinforced Plastic Composites. *Compos. Sci. Technol.* **2017**, *147*, 62−70.
(62) Schneider, L. M.; Ihrner, N.; Zenkert, D.; Johansson, M. Bicontinuous Electrolytes via Thermally Initiated Polymerization for Structural Lithium Ion Batteries. *ACS Appl. Energy Mater.* **2019**, *2*, 4362−4369.
(63) Johannisson, W.; Harnden, R.; Zenkert, D.; Lindbergh, G. Shape-Morphing Carbon Fiber Composite using Electrochemical Actuation. *Proc. Natl. Acad. Sci. U. S. A.* **2020**, *117*, 7658−7664.
(64) Liu, F.; Shi, Z.; Dong, Y. Improved Wettability and Interfacial Adhesion in Carbon Fibre/Epoxy Composites via an Aqueous Epoxy Sizing Agent. *Composites Part A: Applied Science and Manufacturing* **2018**, *112*, 337−345.
(65) Liang, H.; Zuo, X.; Zhang, L.; Huang, W.; Chen, Q.; Zhu, T.; Liu, J.; Nan, J. Nonflammable LiTFSI-Ethylene Carbonate/1,2-Dimethoxyethane Electrolyte for High-Safety Li-ion Batteries. *J. Electrochem. Soc.* **2020**, *167*, No. 090520.
(66) Weng, A.; Mohtat, P.; Attia, P. M.; Sulzer, V.; Lee, S.; Less, G.; Stefanopoulou, A. Predicting the Impact of Formation Protocols on Battery Lifetime Immediately After Manufacturing. *Joule* **2021**, *5*, 2971−2992.
(67) Moretti, A.; Sharova, V.; Carvalho, D. V.; Boulineau, A.; Porcher, W.; de Meatza, I.; Passerini, S. A Comparison of Formation Methods for Graphite//LiFePO4 Cells. *Batteries Supercaps* **2019**, *2*, 240−247.
(68) Jeong, D.; Yook, J.; Hong, D. G.; Lee, J.-C. Lithium Dendrite Suppression by Single-Ion Conducting Gel Polymer Electrolyte Cross-Linked with Graphene Oxide. *J. Power Sources* **2022**, *534*, No. 231424.
(69) Khurana, R.; Schaefer, J. L.; Archer, L. A.; Coates, G. W. Suppression of Lithium Dendrite Growth Using Cross-Linked Polyethylene/Poly (ethylene oxide) Electrolytes: A New Approach for Practical Lithium-Metal Polymer Batteries. *J. Am. Chem. Soc.* **2014**, *136*, 7395−7402.

https://doi.org/10.1021/acsami.4c08698
ACS Appl. Mater. Interfaces 2024, 16, 59128−59142